09

Raman and Photoluminescence Spectra for Yb and Lu doped the Strontium Zirconate $SrZrO_3$

© S.N. Shkerin[1], A.V. Pavlovich[1], R.K. Abdurakhimova[1], T.V. Yaroslavtseva[2], E.S. Ul'yanova[2]

[1] Institute of High-Temperature Electrochemistry, Ural Branch, Russian Academy of Sciences, Yekaterinburg, Russia
[2] Institute of Solid State Chemistry, Russian Academy of Sciences, Ural Branch, Yekaterinburg, Russia

E-mail: shkerin@mail.ru

Received January 31, 2024
Revised January 31, 2024
Accepted February 5, 2024

Raman spectra equipment with different wavelengths (532 and 785 nm) was used for investigation of derivatives based on strontium zirconate. A number of reflexes independent of the laser wavelength are identified as the structure related. Sr−O vibration observed at 93 cm^{-1} is previously discussed in detail in the literature and it is generally accepted that it realizes at the smallest wave numbers. The presence of the 59 cm^{-1} structure band is shown at first time. It is interpreted as manifestation of vibration of a heavy cation in the strontium position (Lu_{Sr})−O. Reflexes that depend on the laser wavelength are considered as related to luminescence. It was evidenced an oxygen vacancies self-manifestation by luminescence using the dependence of line intensity on material composition. It was first time observed for materials with perovskite structure in this study.

Keywords: Perovskite structure, $SrZrO_3$, Raman spectroscopy, pointe defects associates luminescence.

DOI: 10.61011/PSS.2024.03.57943.12

1. Introduction

Perovskite-structure oxides are actively studied since 1980s, when Ivahara et al. detected proton conductivity in acceptor doped strontium cerates at the high temperatures (> 600°C) [1–4]. After that, the proton transfer capability was also detected in other perovskite-structure oxides and derivatives thereof [5–15]. The high-temperature proton electrolytes are of interest due to high-efficient electrochemical systems for generation of electrical energy, hydrogen production, gas analysis, etc., to be created based thereon [16–19]. High proton conductivity is typical for perovskites based on barium and strontium cerates, but they are subject to fast degradation due to formation of hydroxides and carbonates when interacting with water vapor and carbon dioxide in the atmosphere [6,8,20–22]. Besides, cerates have significant electron conductivity, thereby resulting in reduced Faraday efficiency of the electrochemical processes [23]. Unlike cerates, zirconates of alkaline earth elements are characterized by hich chemical stability as well as high ion transfer numbers [24–29], which is necessary for application in the electrochemical systems; but conductivity of zirconates is not high. In this regard, the capabilities are still searched for improving ion conductivity of zirconates, including by acceptor doping, varying cation stoichiometry, creating composites/nanocomposites, etc. [7,8,24–27,29–35]. All these approaches are aimed at changing a defect structure of the crystals, which defines the ion conductivity. For deeper understanding the mechanisms of „tuning" the transport properties, it is highly important to study a local structure of zirconates.

There are not so many methods of short-range order research, and some of them are not readily available [36]. The most common method for studying the local structure is vibrational spectroscopy. Earlier, based on analysis of Raman scattering (RS) spectra of the series of the samples $Sr_xZrO_{3-\delta}$ and $Sr_xZr_{0.95}Y_{0.05}O_{3-\delta}$ ($x = 0.94-1.00$), we have established that strontium deficiency promoted filling the strontium position by dopant cations [37]. The cations of yttrium, strontium and zirconium have similar weights, thereby making it impossible to apply other methods, for example, X-ray diffraction, for solving this task. The presence of the defects Y_{Sr} (Y_{Sr} designates a substitution defect – yttrium cation in the strontium position) is proved by a broadened line 93 cm^{-1}, which corresponds to the Sr−O valence vibration. If our developed representations are true, then introduction of a more bulky cation M into strontium zirconate as a dopant will result not in the broadened line corresponding to the Sr−O valence vibration, bur rather to appearance of an additional band due to the M_{Sr}−O vibration.

Exemplified by oxides with a fluorite structure, the studies [38–40] have shown that RS spectroscopy enabled detecting luminescence of oxygen vacancies, which are a principal intrinsic property of oxide solid electrolytes. Such studies are not known for the perovskite-structure materials, so the present study will be aimed thereat. The studies were on the lutetium-doped strontium zirconate samples $SrZr_{1-x}Lu_xO_{3-\delta}$ ($x = 0.03-0.10$) and the solid solutions $Sr_xZr_{0.95}Yb_{0.05}O_{3-\delta}$ ($x = 0.94-1.00$), which contain ytterbium, whose production and certification are described earlier [33,35].

2. Experimental part

The production and certification of the lutetium-doped strontium zirconate samples $SrZr_{1-x}Lu_xO_{3-\delta}$ are detailed in [35]. The powders $SrZr_{1-x}Lu_xO_{3-\delta}$ ($x = 0.03$, 0.05, 0.07, 0.10) (hereinafter referred to as Lu3−Lu10) have been synthesized by a chemical solution method from precursors $SrCO_3$, $ZrO(NO_3)_2 \cdot H_2O$ and Lu_2O_3, which have purity of 99.9%. The calculate amounts of the powders $SrCO_3$ and Lu_2O_3 were introduced into the aqueous solution of zirconyl nitrate and slowly heated to obtain a transparent solution. Then, a complexing agent — citric acid, was introduced, so was glycine as fuel. The molar ratio of the ions of the metals, glycine and citric acid was 2 : 2 : 1. The mixture was evaporated at the temperature of 90°C with periodic stirring until self-ignition. The obtained powder was being synthesized at 1300°C for 2 h, then ground and pressed in tablets at the pressure of 300 MPa and baked at 1650°C for 5 h. The samples have been investigated by the methods of X-ray diffraction, electron microscopy and energy-dispersive X-ray microanalysis to show that at the lutetium content of 3 mol.% a single-phase sample with the rhombic structure $SrZrO_3$ was obtained, while at the higher dopant concentrations the impurity phase with the high content of lutetium appeared.

Production and certification of the ytterbium-doped strontium zirconate samples $Sr_xZr_{0.95}Yb_{0.05}O_{3-\delta}$ ($x = 0.94$, 0.96, 0.98, 1.00) (hereinafter referred to as Sr94−Sr100) are described in [33]. The precursors $ZrO(NO_3)_2 \cdot 2H_2O$, $Yb(NO_3)_3 \cdot nH_2O$ and $SrCO_3$ were used for the synthesis by the chemical solution method. First, individual solutions were prepared: zirconyl nitrate in distilled water and ytterbium nitrate hydrate in ethanol, then the solutions were merged and the powder $SrCO_3$ in a calculated ratio was added. Glycine and citric acid were introduced into the obtained mixture (the ratio of the ions of the metals, glycine and citric acid 2 : 2 : 1). The solution was held at the temperature of 90°C with periodic stirring until self-ignition. The obtained powder was annealed at 1200°C for 2 h, then ground, pressed in tables and baked at the temperature of 1600°C for 1 h. The samples were certified by the methods of X-ray diffraction, electron microscopy and energy-dispersive X-ray microanalysis. As a result, it has been established that the samples Sr96−Sr100 are of a single phase and have the rhombic structure, while the sample Sr94 exhibits the impurity phase based on zirconium dioxide.

Purity of the reagents Lu_2O_3 and $Yb(NO_3)_3 \cdot nH_2O$ was monitored by the method of atom-emission spectrometry with inductively coupled plasma by means of the instrument Optima 4300 DV produced by PerkinElmer (USA). The results are shown in Tables 1 and 2.

For the lutetium oxide, attention is paid to impurities of gadolinium and ytterbium (Table 1). Although their concentration is low, but since sensitivity of the optical methods to radiation recording is high, below we can see small-intensity ytterbium lines. The gadolinium cation has no active line within an area of the studied conditions. For the ytterbium oxide, the detected impurities are not optically active in the conditions of this study.

Table 1. Results of determination of the cation composition of Lu_2O_3 by the method of atom-emission spectrometry with inductively coupled plasma

	Element	wt%
1	Lu	83.17
2	Gd	0.053
3	Yb	0.0082
4	Si	0.043

Table 2. Results of determination of the cation composition of $Yb(NO_3)_3 \cdot nH_2O$ by the method of atom-emission spectrometry with inductively coupled plasma

	Element	wt%
1	Yb	87.88
2	Ca	0.022
3	Fe	0.003
4	Mn	0.0005
5	Ni	0.0011
6	Si	0.052
7	Zr	0.0045

The studies by Raman scattering method were performed using two instruments:

− in green radiation ($\lambda = 532$ nm) on the equipment Renishaw U 1000 microscope-spectrometer; power of the Nd : YAG laser was 50 mW;

− in red radiation ($\lambda = 785$ nm) on InVia Reflex with the microscope Leica DM2700; power of the Renishaw diode laser with an integrated plasma filter was 300 mW.

The signal accumulation time was from 10 to 30 s, while the number of scans was from 5 to 16.

3. Results

3.1. Ytterbium-doped strontium zirconate

In order to investigate by the RS spectroscopy, just before the experiment, the ceramic sample was broken apart and spectra of new cuts were recorded, since the method is sensitive to the surface adsorbed impurities. Theoretically, the spectrum of strontium zirconate having a rhombic symmetry contains 24 RS-active modes, which include 7 modes A_g, 5 modes B_{1g}, 7 modes B_{2g} and 5 modes B_{3g}, are observed within the range of wave numbers 94−777 cm^{-1} [41]. The results obtained on the new cuts of the ceramic samples $Sr_xZr_{0.95}Yb_{0.05}O_{3-\delta}$ using the green laser (the wave length 532 nm) are shown on Figure 1. As can be seen, the area of the small wave numbers (below 116−118 cm^{-1}) can not be recorded. This

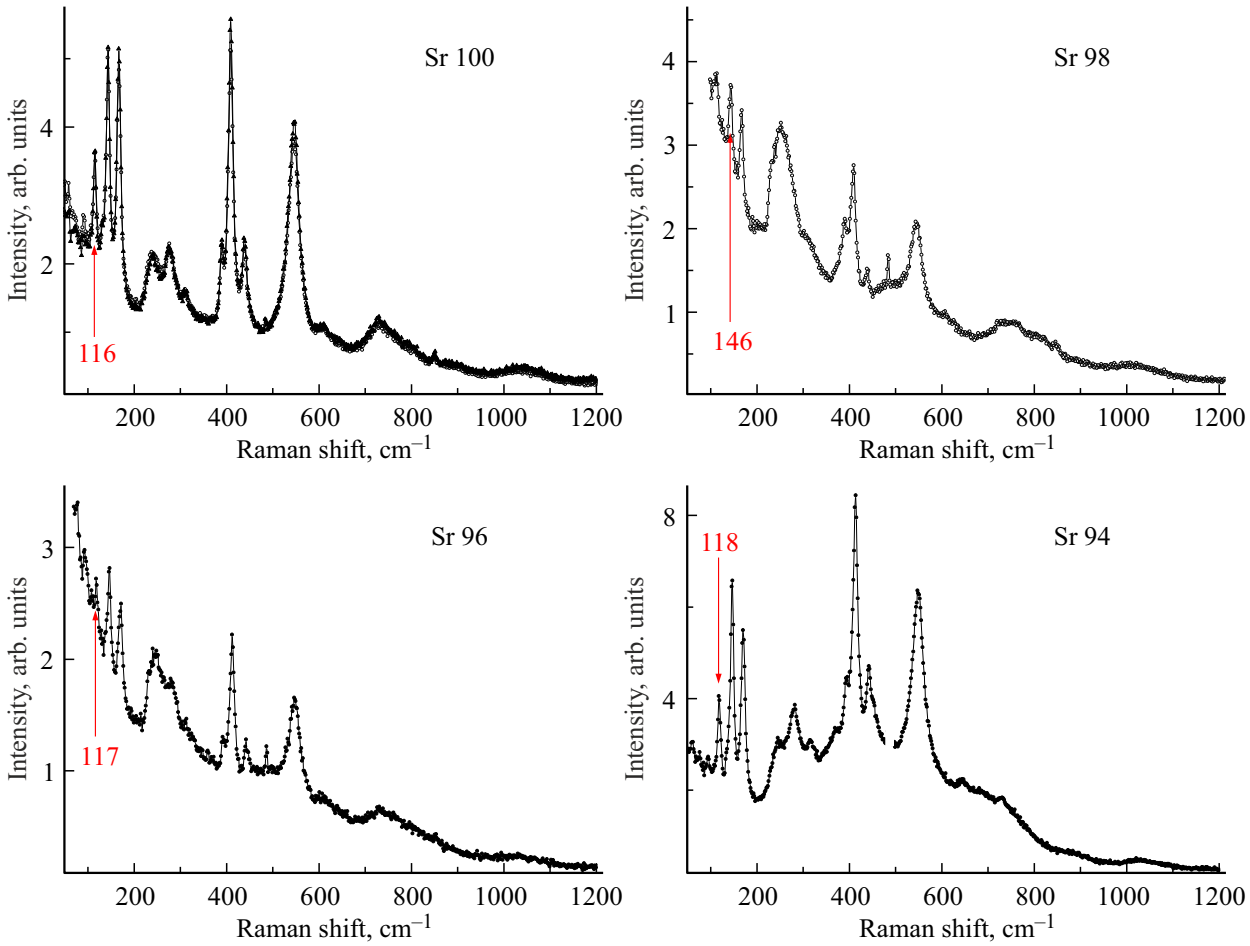

Figure 1. RS-spectra of $Sr_xZr_{0.95}Yb_{0.05}O_{3-\delta}$, which are obtained using the green (532 nm) laser.

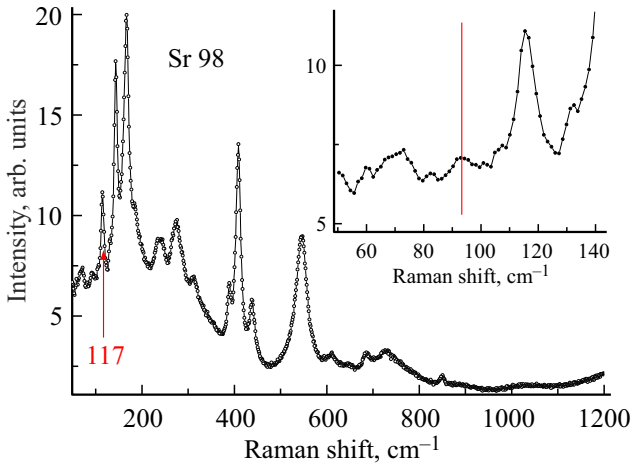

Figure 2. RS-spectrum of the sample Sr98, as obtained using the red (785 nm) laser. The vertical line of the inset marks the band 93 cm^{-1}.

problem is solved by using the red (785 nm) laser; the obtained spectra are shown on Figure 2. The inset clearly shows the line 93 cm^{-1}, which corresponds to the Sr–O valence vibration (the A_g-mode is marked by a vertical dashed line) and reflexes to the left of it. In accordance with both the theoretical study [41], and some experimental studies [37,42–45], no line should be observed within the area of the small wave numbers (below 93 cm^{-1}).

The reflexes observed to the left of the line 93 cm^{-1} can correspond to the Yb_{Sr}–O vibration (Yb_{Sr} means the ytterbium cation in the strontium cation position), which is shifted in relation to the line Sr–O due to the large mass of he ytterbium cation (the masses f the atoms of strontium and ytterbium are 87.62 and 173.04 Da, respectively), or photoluminescence caused by presence of structural defects. It is possible to distinguish photoluminescence and Raman scattering using excitation sources of a various wavelength. A position of the Raman scattering lines does not depend on the source wavelength, whereas the position of the photoluminescence lines changes depending on the source quantum energy. The solution of a problem for separating the lines, which correspond to Raman scattering and photoluminescence, has been recently exemplified for oxide materials with the fluorite structure [38–40].

The Figures 3 and 4 show the spectra obtained using the green and the red laser within the area of the high wave

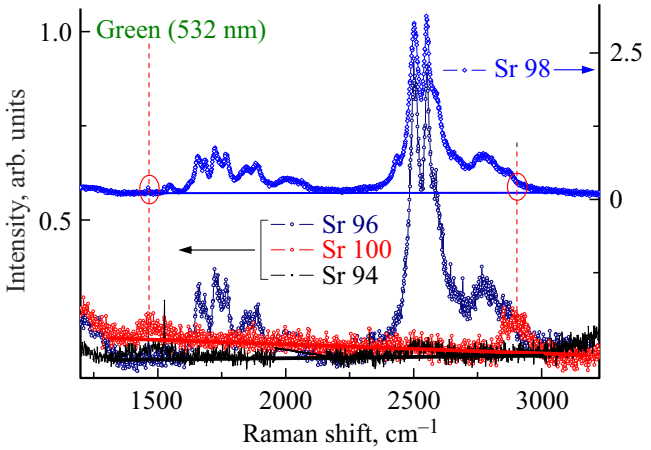

Figure 3. RS-spectra of $Sr_xZr_{0.95}Yb_{0.0}5O_{3-\delta}$ within the area of the wave numbers 1250−3250 cm^{-1}, which are obtained using the green (532 nm) laser.

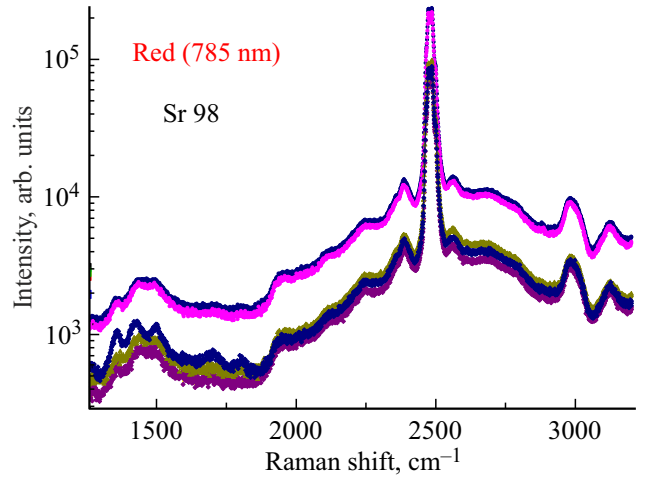

Figure 4. RS-spectra of the sample Sr98 within the area of the wave numbers 1250−3250 cm^{-1}, which are obtained using the red (785 nm) laser.

numbers (1250−3250 cm^{-1}). The intense lines obtained using the red laser were expected, since this area contains the luminescence lines of the ytterbium cation [46–48]. The intensity of the line is extremely high, thereby necessitating the use of a logarithmic scale. There are unexpected results obtained using the green laser: the sample Sr98 exhibits quite intense bands (Figure 3). Figure 5 shows the spectra of this sample, which are obtained using the green and the red laser. The lines observed in the different radiations do not coincide and, therefore, are manifestation of luminescence. For the sample Sr96 the intensity of these bands noticeably decreases (Figure 3). For the samples Sr94 and Sr100, even at the long signal accumulation time, the spectra exhibit only two weak reflexes near 1465 and 2884 cm^{-1} (they are marked on Figure 3), which will be discussed by us below.

Photoluminescence due to anion vacancies is well known, but predominantly for materials with the fluorite structure [39,40,49–51]. As far as we know, for the oxides with the perovskite structure, no luminescence of the oxygen vacancies is reported. Figure 6 shows the photoluminescence spectrum of the composition Sr98, as calculate to the wavelength, which is more accepted for optical studies. For conversion between the spectral wavelength and the wave numbers of the shift in the RS spectrum, the following formula has been used:

$$\Delta\nu = \frac{c}{\lambda_0} - \frac{c}{\lambda_1}, \qquad (1)$$

where $\Delta\nu$ — the spectral shift expressed in the wave number, λ_0 — the excitation wavelength, λ_1 — the wavelength of the spectrum, c — the speed of light.

Within the area of intrinsic luminescence of the ytterbium cation, we have decomposed the observed spectra into the set of Gaussian-shaped lines, using the previously described procedure [38–40]. Figure 7 shows such decomposition for a part of the spectrum of the sample Sr98 within the area of

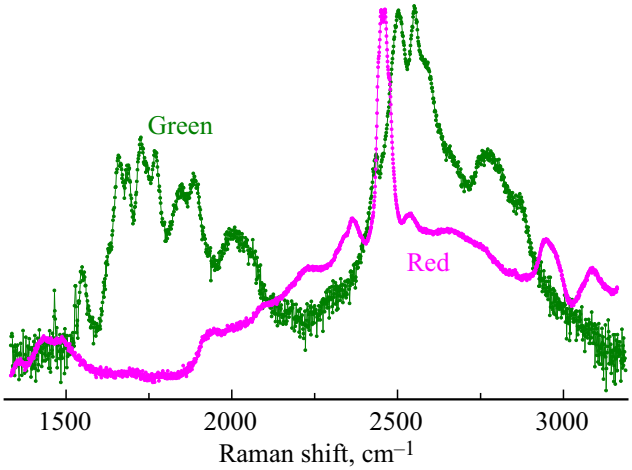

Figure 5. RS-spectra of the sample Sr98, which are obtained in the red and green lasers within the area of the wave numbers 1250−3250 cm^{-1}.

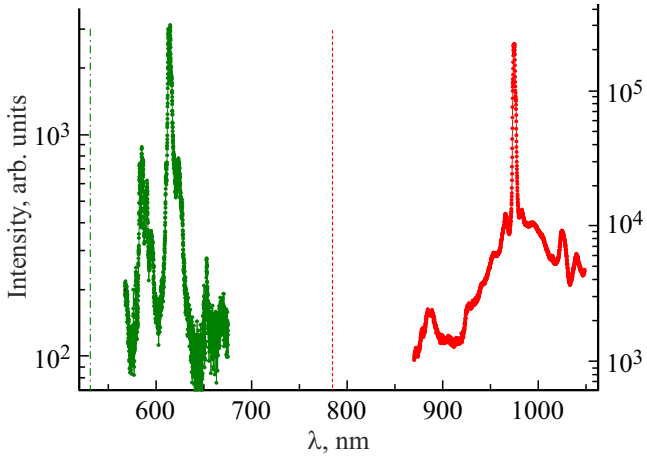

Figure 6. Photoluminescence of the sample Sr98. The vertical lines show the excitation radiation wavelength.

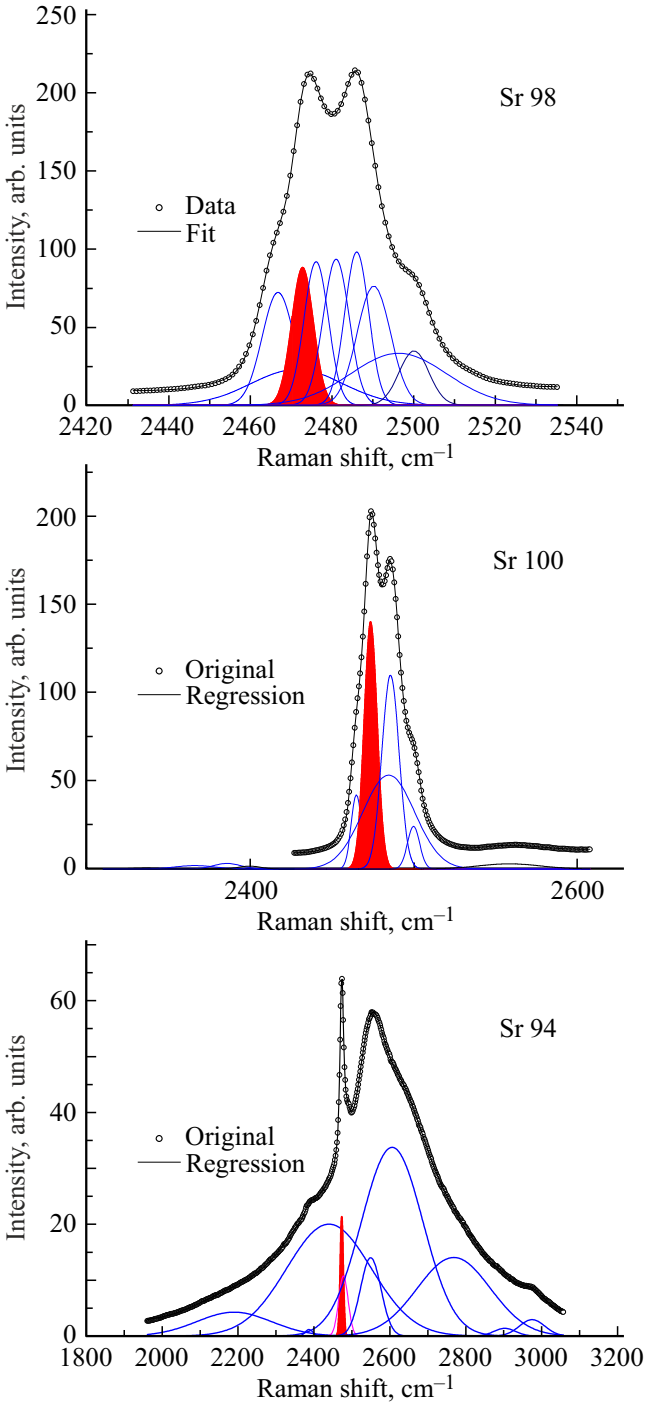

Figure 7. Decomposition of the spectra shot in the red (786 nm) laser into a set of Gaussian-shaped lines for the samples: Sr98, Sr100, Sr94. The upper part of the figure (Sr98) shows a difference curve between the experimental and the fitting spectrum. The shaded line corresponds to the luminescence band of the ytterbium cation.

the wave numbers 1250−3250 cm^{-1}. The upper part of the figure shows a difference curve between the experimental and the fitting spectrum. Figure 7 also shows similar results for the samples Sr100 and Sr94. It can be seen that only the line 2472 ± 1 cm^{-1} is invariant (highlighted in red), it is a line of ytterbium luminescence. Usually, for ytterbium luminescence a triplet is observed [39,40,46–48]. But, in this case the ytterbium concentration is low, whereas intensity of the satellite lines is below the basic line by an order, so it is difficult to distinguish them against the background of other effects. Thus, when irradiating by the red laser, the ytterbium main line in a strontium zirconate matrix is observed at 2472 ± 1 cm^{-1}.

3.2. Lutetium-doped strontium zirconate

The Figures 8 and 9 show the RS spectra of the samples $SrZr_{1-x}Lu_xO_{3-\delta}$, which are obtained using the green and the red laser. The area of the wave numbers up to 1200 cm^{-1}, which usually exhibit the Raman scattering lines, the spectra are similar to the spectra of the samples $Sr_xZr_{0.95}Yb_{0.05}O_{3-\delta}$, as shown on the figures 1 and 2. The difference lies in the very high intensity of the lines within the area 700−900 cm^{-1} (they are highlighted by a dashed frame on the figures 8 and 9) in comparison with the spectra $Sr_xZr_{0.95}Yb_{0.05}O_{3-\delta}$, and the spectra $Sr_xZr_{0.95}Y_{0.05}O_{3-\delta}$, as given in the study [37]. The figures 8 and 9 also show the spectra for the area of the wave numbers 900−4999 cm^{-1}; they exhibit the bands that are commonly related luminescence.

As we have noted above, it is possible to separate the bands caused by luminescence and Raman scattering by using the sources of a different wavelength. Figure 10 shows decomposition of the spectra of the sample Lu3, which are obtained using the green and the red laser, within the area of the small wave numbers. The black color highlights the bands, which do not depend on the wavelength of the excitation source. Among them, there is a band 93 cm^{-1} that corresponds to the Sr−O valence vibration, and the band 59 cm^{-1}, which could not be recorded by us for the ytterbium-doped sample due to the green laser's problems (Figure 1). It follows from analysis of the spectra of the samples $SrZr_{0.97}Lu_{0.03}O_{3-\delta}$ that the band 59 cm^{-1} corresponds to Raman scattering, since its position is the same while varying the wavelength of the excitation radiation. We believe that this is Lu_{Sr}−O valence vibration (Lu_{Sr} designates the lutetium cation in the strontium cation position), which is shifted to the area of the smaller wave numbers in comparison with the Sr−O vibration due to a much bigger mass of lutetium (the lutetium atom mass is 174.97 Da). The bands, which are highlighted by the red and the green color on Figure 10, are either shifted or disappear when the radiation source is replaced; therefore, they are caused by photoluminescence.

Figure 11 shows the wave numbers of the Raman scattering lines $SrZr_{1-x}Lu_xO_{3-\delta}$ depending on the lutetium concentration. The data for the undoped $SrZrO_3$ and interpretation of the vibrational modes have been taken from the study [37]. The shaded characters show lines, which are observed both for the undoped and the doped samples. Some of them quickly disappear when doping, for example,

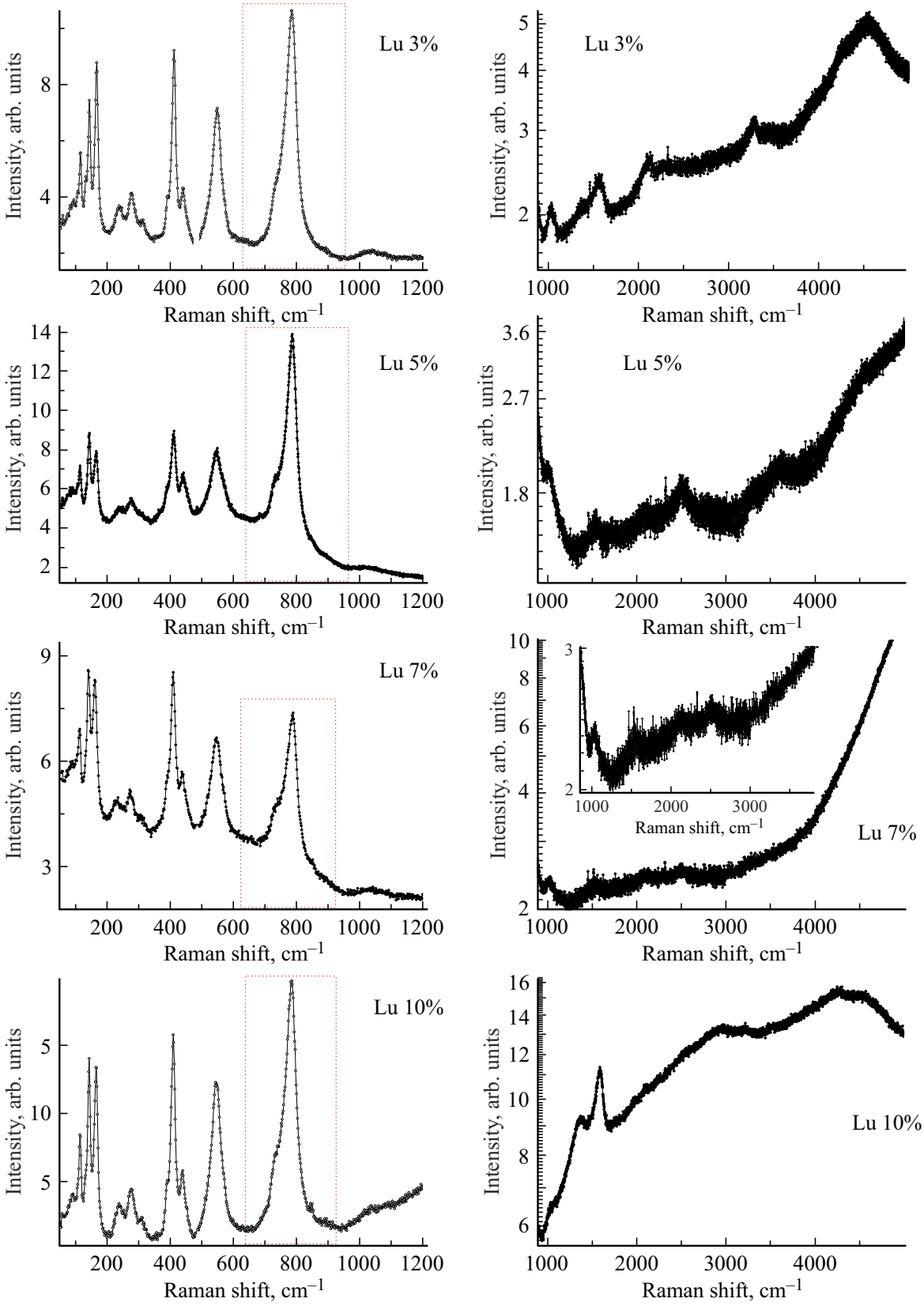

Figure 8. RS-spectra of the samples $SrZr_{1-x}Lu_xO_{3-\delta}$, which are obtained using the green (532 nm) laser.

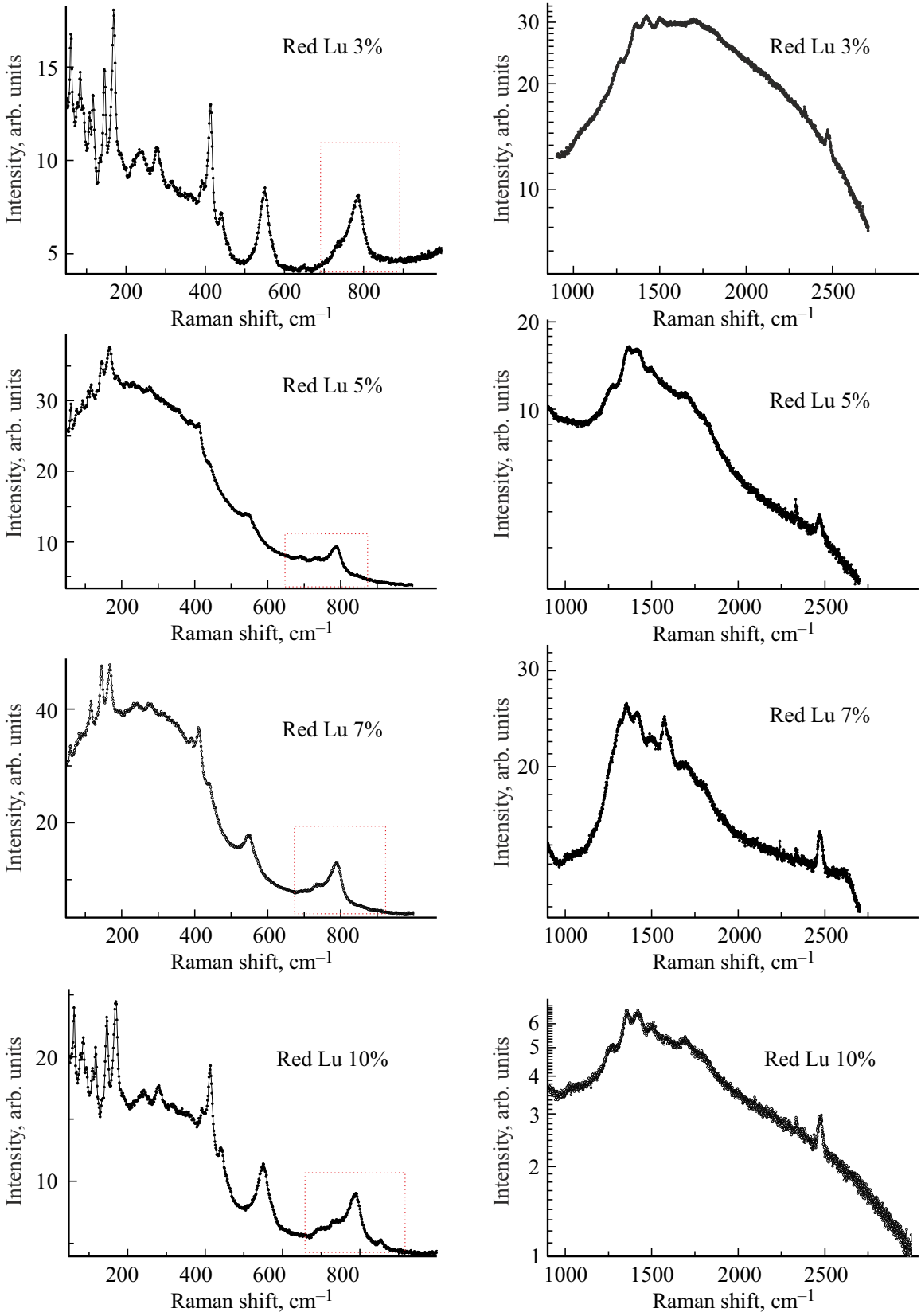

Figure 9. RS-spectra of the samples $SrZr_{1-x}Lu_xO_{3-\delta}$, which are obtained using the red (785 nm) laser.

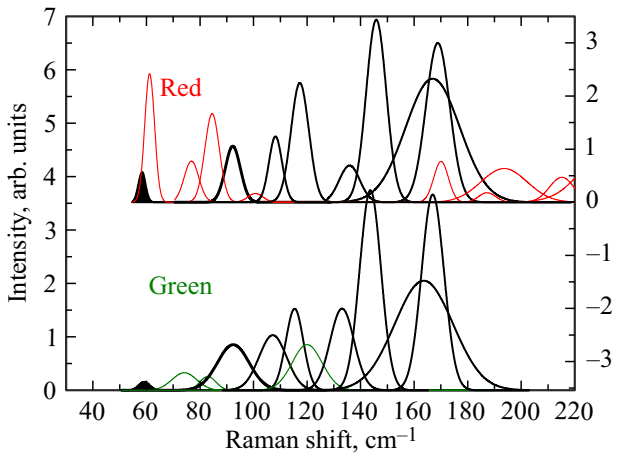

Figure 10. Decomposition of the spectra of the sample Lu3, which are obtained using the red (the right ordinate) and the green (the left ordinate) laser. The black color highlights the bands, which do not depend on the wavelength of the radiation source.

B_{1g} at 775 cm^{-1} and $B_{1g/3g}$ at 134.5 cm^{-1}. Another part of the lines appears with introduction of a dopant, for example, the mode Ag at 59 cm^{-1} that corresponds to the LuSr−O valence vibration; these lines are shown by unshaded characters. The lines *1′* and *2′* within the area ~ 800 cm^{-1} appear only for the doped material, but, we believe, they are similar to the lines *1* (B_{3g} 708 cm^{-1}) and *2* (B_{2g} 750 cm^{-1}) for the undoped material, which will be discussed by us later.

Figure 12 shows decomposition of the spectra of the sample Lu5, which are obtained using the red and the green laser, within the area of the big wave numbers. The band 1525 cm^{-1} (it is highlighted in black) corresponds to Raman scattering, since it does not depend on the wavelength of the excitation radiation. In accordance with the simulation representations [41], no first-order reflex can be observed within this area of the wave numbers. The similar vibrational mode 1488 cm^{-1} is observed for the composition Lu3, but it lacks for the compositions with Lu7 and Lu10. Existence of the Raman scattering high-order bands has been previously reported for a material based on zirconium dioxide [39] and diamonds [52]. Presently, there is no common representation about reasons of appearance thereof. But, apparently, the high-order bands appearance reflects peculiarities of covalence bonding between the cations inside the material. The two weak reflexes of the spectra of the ytterbium-doped strontium zirconate, 1465 and 2884 cm^{-1}, shown on Figure 3, probably, also correspond to the Raman scattering high-order lines; one

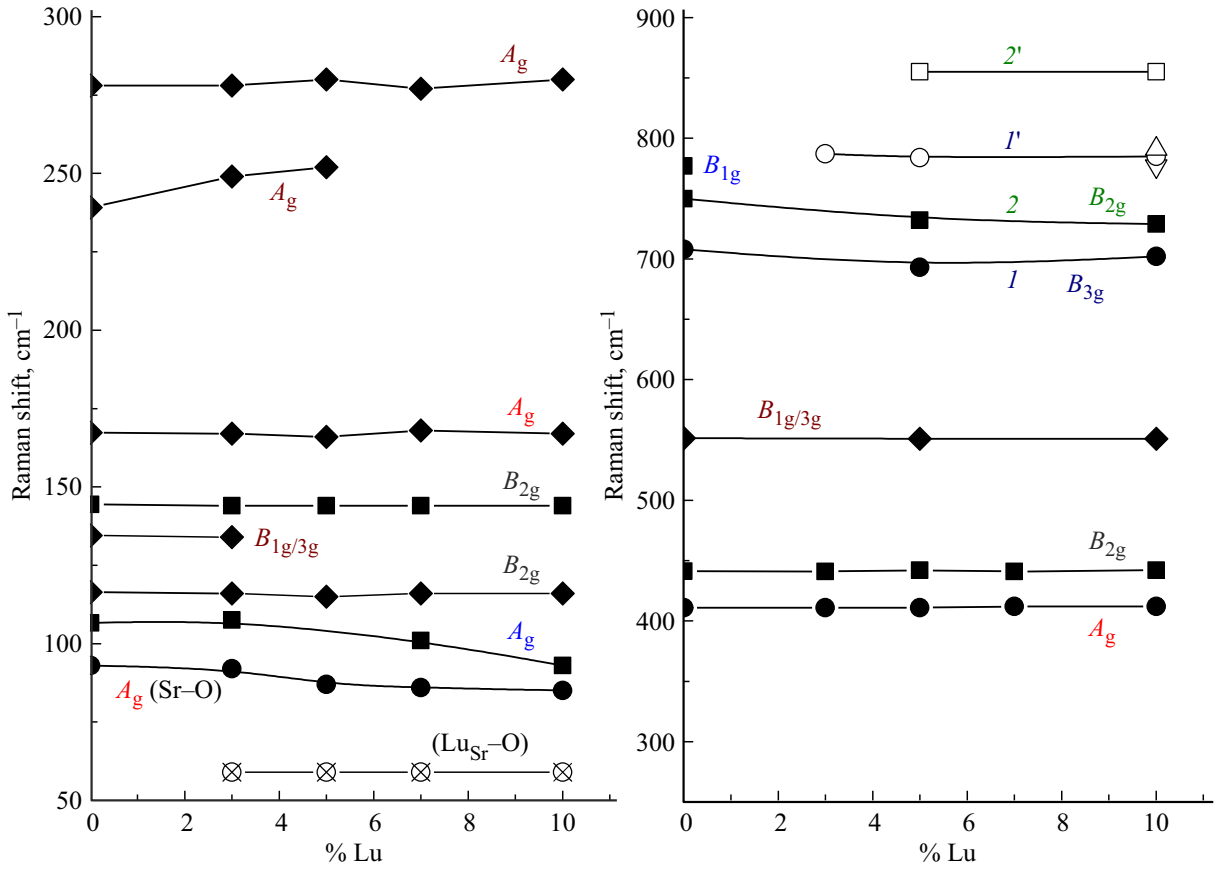

Figure 11. Dependence of frequencies of manifestation of the stokes (not depending on the wavelength of the radiation source) lines on the lutetium concentration. Data for the lutetium zero concentration is taken from Table 3 of the study [37], which shows a band correlation as well.

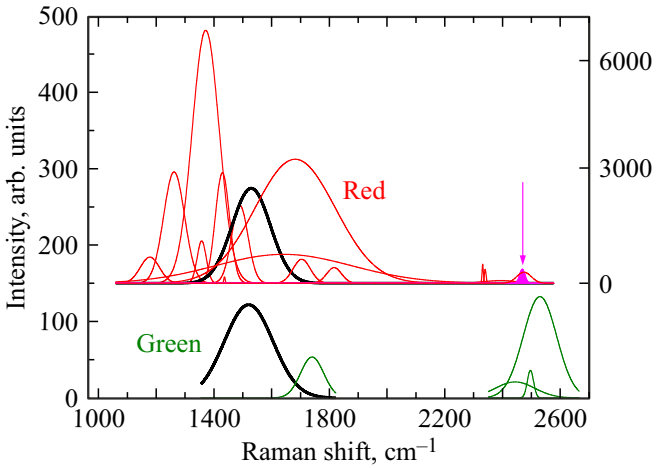

Figure 12. Decomposition of the spectra of the sample Lu5, which are obtained using the red (the right ordinate) and the green (the left ordinate) laser. The black color highlights the bands, which do not depend on the wavelength of the radiation source. The arrow marks the Yb luminescence line.

of them ($1465\,\text{cm}^{-1}$) is near the band observed for the lutetium-doped strontium zirconate ($1488-1525\,\text{cm}^{-1}$). But in case of ytterbium we failed to definitely highlight the stokes lines.

Figure 12 shows the low-intensity band (it is shaded in red and marked with an arrow). These bands are clearly observed in the logarithmic coordinates, too (see Figure 9). Their frequencies correspond to ytterbium luminescence. The additional studies of the chemical compositions of the initial reagents (Table 1) have shown presence of small quantities of the ytterbium cations in the lutetium reagent. Due to the small concentration of the ytterbium impurity, we observe only the most intense one of the triplet lines. Its satellites usually have intensity of at least one order below [39,40,46].

4. Discussion

4.1. Oxygen vacancies as the luminescence source

The results of Figure 3 show substantial change of the spectra of the samples $Sr_xZr_{0.95}Yb_{0.05}O_{3-\delta}$ ($x = 0.94-1.00$) with relatively small variation of the strontium content. Since the wave numbers of the lines of Figure 3 depend on the wavelength of the excitation radiation, then these lines can be considered to be manifestation of luminescence. The most probable centers of luminescence are oxygen vacancies. We have previously studied influence of nonstoichiometry of strontium on the transport properties of the zirconates $Sr_xZr_{0.95}Yb_{0.05}O_{3-\delta}$ ($x = 0.94-1.00$) [33,34]. Substitution of zirconium with ytterbium in strontium zirconate results in formation of acceptor defects Yb'_{Zr}, whose charge is compensated by the oxygen vacancies; it is a known method of acceptor doping, which is used to increase ion conductivity of the oxides. It has been established that ion conductivity of the samples with slight deficiency of strontium (Sr98) increased in comparison with the stoichiometric sample, but further reduction of the strontium content resulted in the reduced conductivity. It was assumed that this conductivity behavior was caused by the fact that with slight deficiency of strontium in the structure of perovskite $Sr_xZr_{0.95}Yb_{0.05}O_{3-\delta}$ the charge of the strontium vacancies was compensated by formation of additional oxygen vacancies, thereby ensuring the increased ion conductivity; but increase in the strontium deficiency stimulates filling of its positions with ytterbium cations, which in this case are a donor impurity, and in order to retain electrical neutrality the concentration of the oxygen vacancies decreased. The mechanism of formation of the defects in $Sr_xZr_{0.95}Yb_{0.05}O_{3-\delta}$ is detailed in [34]. Thus, the maximum number of the oxygen vacancies is achieved for the composition Sr98. There is similar variation of intensity of the luminescence lines of the samples $Sr_xZr_{0.95}Yb_{0.05}O_{3-\delta}$ (Figure 3), thereby enabling considering the oxygen vacancies as the luminescence centers.

The results of Figure 4 can be interpreted as manifestation of photoluminescence of the oxygen vacancies. There are two wide bands observed: within the area $1200-1700\,\text{cm}^{-1}$, which corresponds to the wavelengths 880–900 nm (Figure 6), and within the area $1900-3200\,\text{cm}^{-1}$, which corresponds to the wavelengths 960–990 nm for the maximum position (Figure 6). The same frequency area exhibits a line of intrinsic luminescence of the ytterbium cation ($2472 \pm 1\,\text{cm}^{-1}$ at the excitation radiation wavelength 785 nm), but, as shown on the figures 7 and 8, it is not the only one.

4.2. Comparison of the properties of strontium zirconates, which are doped with ytterbium and lutetium

Comparison of the spectra $SrZr_{1-x}Lu_xO_{3-\delta}$ and $Sr_xZr_{0.95}Yb_{0.05}O_{3-\delta}$ within the area of the big wave numbers (the figures 4 and 9) shows the presence of the same bands. Only in case of ytterbium doping intensity of the lines within the area 960–990 nm (which corresponds to $1900-3200\,\text{cm}^{-1}$ on the figures 4 and 9) is much higher than intensity of the lines within the area 880–900 nm (which corresponds to $1200-1700\,\text{cm}^{-1}$ on the figures 4 and 12), and it is vice versa in case of lutetium doping (Figure 9).

Another obvious difference of the zirconates doped with ytterbium and lutetium is significant difference of intensity of the bands within the area $650-900\,\text{cm}^{-1}$ (Figure 1, 2, 9, 11); the said area is highlighted by red frames. Substantial redistribution of intensity of the Raman scattering lines reflects variation of the local structure.

5. Conclusion

Using the samples of the solid solutions based on strontium zirconate (whose production and certification have been previously detailed), their optical characteristics have been studied using the Raman spectrometers with lasers of the different wavelength (532 and 785 nm). Comparison of the results obtained using the various sources enables separating the lines, which reflects the structure from the lines corresponding to luminescence.

In the studied materials, luminescence is caused by associates of the defects based on the oxygen vacancies, which is well illustrated by Figure 3 showing appearance of the reflexes when the oxygen vacancies appear. The wavelengths of these bands are about 585 and 620 nm (Figure 6). In addition to these lines detected using the green laser, all the studies samples exhibit the bands at the wavelengths 885 nm and the wide band or the set of the bands at 980 nm detected using the red laser. The intensity ration of these bands is different for the lutetium-doped material and the materials doped with ytterbium and yttrium.

There are identified structural reflexes as non depending on the wavelength of the excitation laser. In general, the obtained results well agree with those previously obtained for yttrium-doped strontium zirconate and with other literature data (Figure 11). It was the first time to show presence of the band 59 cm^{-1}, which is interpreted as manifestation of vibration of the heavy cation in the strontium position $(Lu_{Sr})-O$. The Sr−O vibration observed at 93 cm^{-1} previously detailed in the literature is commonly believed to be realized at the smallest wave numbers.

Acknowledgments

The authors would like to thank N.I. Moskalenko for specification of the chemical composition of the oxides of lutetium and ytterbium and L.A. Dunyushkina for provision of the samples and constructive discussion of a manuscript of this paper.

Funding

The study was carried out within the framework of the budget financing program (the topic registration number 122020100209-3) at the IVTE UrO RAS.

The study was performed using the equipment of the collective use of the Institute of High-Temperature Electrochemistry of the Ural Branch of the Russian Academy of Sciences.

Conflict of interest

The authors declare that they have no conflict of interest.

References

[1] H. Iwahara, T. Esaka, H. Uchida, N. Maeda. Solid State Ionics **3**−**4**, 359 (1981).
[2] H. Iwahara, H. Uchida, S. Tanaka. Solid State Ionics **9**−**10**, *Part 2*, 1021 (1983).
[3] H. Iwahara, H. Uchida, N. Maeda. J. Power Sources **7**, *3*, 293 (1982).
[4] T. Takahashi, H. Iwahara. Rev. Chim. Miner. **17**, *4*, 243 (1980).
[5] K.D. Kreuer. Annu. Rev. Mater. Res. **33**, 333 (2003).
[6] V.P. Gorelov, V.B. Balakireva, A.V. Kuzmin. Russ. J. Inorg. Chem. **63**, *7*, 930 (2018).
[7] B. Gharbage, F.M.B. Marques, J.R. Frade. J. Eur. Ceram. Soc. **16**, *11*, 1149 (1996).
[8] W. Zajac, D. Rusinek, K. Zheng, J. Molenda. Open Chem. **11**, *7*, 471 (2013).
[9] Z. Shi, W. Sun, Z. Wang, J. Qian, W. Liu. ACS Appl. Mater. Interfaces **6**, *7*, 5175 (2014).
[10] C.Y. Regalado Vera, H. Ding, D. Peterson, W.T. Gibbons, M. Zhou, D. Ding. J. Phys.: Energy **3**, *3*, 032019 (2021).
[11] S. Hossain, A.M. Abdalla, S.N.B. Jamain, J.H. Zaini, A.K. Azad. Renewable. Sustainable Energy Rev. **79**, *C*, 750 (2017).
[12] L.A. Dunyushkina, S.A. Belyakov, N.M. Filatov. J. Eur. Ceram. Soc. **43**, *15*, 6681 (2023).
[13] T. Shimura, M. Komori, H. Iwahara. Solid State Ionics **86**−**88**, *Part 1*, 685 (1996).
[14] J.A. Labrincha, J.R. Frade, F.M.B. Marques. Solid State Ionics **99**, *1*−*2*, 33 (1997).
[15] M. Shiraiwa, T. Kido, K. Fujii, M. Yashima. J. Mater. Chem. A **9**, *13*, 8607 (2021).
[16] S. Choi, C.J. Kucharczyk, Y. Liang, X. Zhang, I. Takeuchi, H.-I. Ji, S.M. Haile. Nature Energy **3**, *3*, 202 (2018).
[17] W. Zhang, Y.H. Hu. Energy Sci. Eng. **9**, *7*, 984 (2021).
[18] L. Lei, J. Zhang, Z. Yuan, J. Liu, M. Ni, F. Chen. Adv. Functional Mater. **29**, *37*, 1903805 (2019).
[19] A.N. Volkov, E.V. Gorbova, A.I. Vylkov, D.A. Medvedev, A.K. Demin, P.E. Tsiakaras. Sensors. Actuators B **244**, 1004 (2017).
[20] K.H. Ryu, S.M. Haile. Solid State Ionics **125**, *1*, 355 (1999).
[21] D.A. Medvedev, J.G. Lyagaeva, E.V. Gorbova, A.K. Demin, P.E. Tsiakaras. Prog. Mater. Sci. **75**, 38 (2016).
[22] Z. Shi, W. Sun, Z. Wang, J. Qian, W. Liu. ACS Appl. Mater. Interfaces **6**, *7*, 5175 (2014).
[23] I. Kosacki, H.L. Tuller. Solid State Ionics **80**, *3*−*4*, 223 (1995).
[24] L. Jiang, T. Norby, D. Han. Chem. Sus. Chem. **16**, *14*, e202300965 (2023).
[25] Z. Tian, F. Ruan, J. Bao, X. Song, S. An, R. Wu, Q. Jing, H.D. Lv, F. Zhou, M. Xie. Electrochem. **166**, *6*, B441 (2019).
[26] J. Bao, Y. Okuyama, Z. Shi, N. Fukatsu, N. Kurita. Mater. Trans. **53**, *5*, 973 (2012).
[27] D.-K. Lim, M.-B. Choi, C.-N. Park, E.D. Wachsman, S.-J. Song. Electrochem. **158**, *3*, B337 (2011).
[28] D. Pérez-Coll, G. Heras-Juaristi, D.P. Fagg, G.C. Mather. Power Sources **245**, 445 (2014).
[29] K. Kato, D. Han, T. Uda. J. Amer. Ceram. Soc. **102**, *3*, 1201 (2019).
[30] S. Imashuku, T. Uda, Y. Nose, K. Kishida, S. Harada, H. Inui, Y. Awakura. J. Electrochem. Soc. **155**, *6*, B581 (2008).

[31] V.B. Balakireva, V.P. Gorelov, L.A. Dunyushkina, A.V. Kuzmin. Phys. Solid State **61**, *4*, 515 (2019).
[32] L.A. Dunyushkina, A.S. Khaliullina, A.N. Meshcherskikh, A.A. Pankratov, D.A. Osinkin. Materials **12**, *8*, 1258 (2019).
[33] A.S. Khaliullina, A.N. Meshcherskikh, A.A. Pankratov, L.A. Dunyushkina. Materials **15**, *12*, 4126 (2022).
[34] A.S. Khaliullina, A.N. Meshcherskikh, L.A. Dunyushkina. Processes **11**, *10*, 2939 (2023).
[35] A.V. Pavlovich, A.A. Pankratov, L.A. Dunyushkina. Membranes **13**, *7*, 663 (2023).
[36] Z. Wang, Z.Q. Chen, J. Zhu, S.J. Wang, X. Guo. Radiation Phys. Chem. **58**, *5–6*, 697 (2000).
[37] S.N. Shkerin, A.V. Rudakova, K.M. Bulanin, A.S. Khaliullina, A.N. Meshcherskikh, E.G. Vovkotrub, L.A. Dunyushkina. Hydrogen Energy **46**, *32*, 17007 (2021).
[38] S.N. Shkerin, E.S. Ul'yanova, E.G. Vovkotrub. Inorg. Mater. **57**, *11*, 1145 (2021).
[39] S.N. Shkerin, E.S. Ulyanova, E.G. Vovkotrub. Phys. Solid State **64**, *4*, 463 (2022).
[40] S.N. Shkerin, A.N. Meshcherskikh, T.V. Yaroslavtseva, R.K. Abdurakhimova. Phys. Solid State **64**, *12*, 1951 (2022).
[41] S. Amisi, E. Bousquet, K. Katcho, P. Ghosez. Phys. Rev. B **85**, *6*, 064112 (2012).
[42] M. Tarrida, H. Larguem, M. Madon. Phys. Chem. Minerals **36**, *7*, 403 (2009).
[43] O. Kamishima, T. Hattori, K. Ohta, Y. Chiba, M. Ishigame. J. Phys.: Condens. Matter **11**, *27*, 5355 (1999).
[44] A. Chopelas. Phys. Chem. Miner. **38**, *9*, 709 (2011).
[45] A. Slodczyk, M.-H. Limage, P. Colomban, O. Zaafrani, F. Grasset, J. Loricourt, B. Sala. Raman Spectroscopy **42**, *12*, 2089 (2011).
[46] Yu.K. Voron'ko, B.I. Denker, V.V. Osiko. FTT **13**, *8*, 2193 (1971). (in Russian).
[47] W.T. Carnall, G.L. Goodman, K. Rajnak, R.S. Rana. J. Chem. Phys. **90**, *7*, 3443 (1989).
[48] C.G. Bünzli, C. Piguet. Chem. Soc. Rev. **34**, *12*, 1048 (2005).
[49] N.G. Petrik, D.P. Taylor, T.M. Orlando. J. Appl. Phys. **85**, *9*, 6770 (1999).
[50] Z. Wang, Z.Q. Chen, J. Zhu, S.J. Wang, X. Guo. Rad. Phys. Chem. **58**, *5–6*, 697 (2000).
[51] J. Costantini, F. Beuneu, M. Fasoli, A. Galli, A. Vedda, M. Martini. J. Phys.: Condens. Matter **23**, 115901 (2011).
[52] S. Prawer, R.J. Nemanich. Phil. Trans. R. Soc. A. **362**, *1824*, 2537 (2004).

Translated by M.Shevelev